JOURNAL OF MATERIALS SCIENCE 13 (1978) 1335–1353

Delayed retardation phenomena of fatigue crack growth in various steels and alloys

S. MATSUOKA, K. TANAKA
Fatigue Testing Division, National Research Institute for Metals, 2-3-12, Nakameguro, Meguroku, Tokyo 153, Japan

The delayed retardation phenomena of fatigue crack growth resulting from a single application of overload were investigated for five steels, two aluminium alloys and a titanium alloy. As long as the small scale yielding condition was satisfied at the overloaded crack tips, the retardation behaviour of these materials was expressed consistently by four parameters; the peak/baseline stress ratio, r, the exponent in the Paris equation, m, the overload-affected zone size, ω_D, and the crack distance at the minimum rate of crack growth, ω_B. Then the parameters, ω_B and ω_D, characterizing the retardation phenomena for these materials were determined. The retardation of aluminium alloys was stronger than that of the other materials. This is attributed to the lower value of ω_B/ω_D in aluminium alloys than in the other materials. In the case of $r = 2$, the overload-affected zone sizes, ω_D, were nearly equal to $1.5\omega_0$ in HT80 steel and aluminium alloys, slightly lower than $1.5\omega_0$ in SNCM8 steel and much larger than $1.5\omega_0$ in A553 steel and the titanium alloy, where ω_0 is the monotonic plastic zone size calculated according to the Dugdale model. The dependence of retardation on baseline stress intensity, ΔK_1, appeared somewhat complicated. In the cases of A553 steel and A2017 aluminium alloy the amount of retardation increased with increasing ΔK_1 value, while in the cases of HT80 steel and Ti–6A1–4V titanium alloy the tendency appeared in the reverse direction. The former behaviour was related to the change in the stress state from plane strain to plane stress at the overloaded crack tips and the latter was related to the threshold of stress intensity.

1. Introduction

The importance of load interaction effects on fatigue crack growth has been well documented. The retardation phenomenon of fatigue crack growth following a single application of overload is one of the fundamental elements of the load interaction effects. In this case, the crack growth rate achieves its minimum value due to the retardation effect, not immediately after the application of the overload, but after the crack has extended a short distance from the point of the overload (see Fig. 1. This phenomenon is referred to as delayed retardation [1]). After the point of minimum growth rate the propagation rate accelerates gradually until it reaches its original growth rate. The retardation phenomena are very complex since they are affected by a large number of variables such as the baseline stress intensity, ΔK_1, the peak/baseline stress ratio, $r = \sigma_2/\sigma_1$, the number of applications of overload, N_p, and material variables [1–7].

The application of the overload results in two effects on the zone ahead of crack tips; the geometric blunting of the crack tip and the formation of a zone of residual compressive stress. The latter tends to close the crack tip but the former tends to open it [2, 3]. The residual compressive stresses influence the relationship between the monotonic and cyclic plastic zones produced ahead of the crack tip propagating at the subsequent baseline load. Matsuoka *et al.* [3] found that the ratios of these two plastic zone

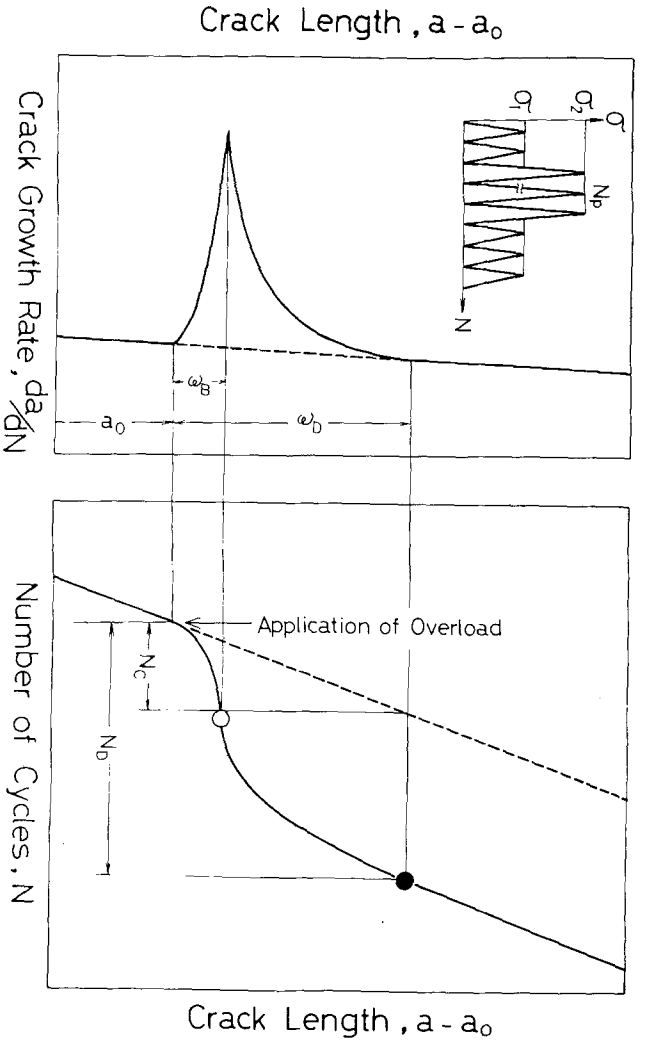

Figure 1 Schematic illustration of delayed retardation phenomenon.

sizes after the overload were just equivalent to those under constant amplitude loading with a stress ratio, $R \equiv \sigma_{min}/\sigma_{max}$, less than zero, and suggested that the resulting crack closure behaviour of a retarding crack could be estimated from those obtained by the constant amplitude testing of an equivalent stress ratio.* They also accounted for the phenomenon of the delayed retardation by assuming that the geometric crack blunting cancels the effect of the residual compressive stresses.

Based on the Paris equation of fatigue crack growth, the retarded crack growth rate, $(da/dN)_D$, is expressed by

$$(da/dN)_D = C_0(\Delta K_{eff})^m = C_0(U_D \Delta K)^m = U_D^m (da/dN)_C \quad (1)$$

where $U_D (= \Delta K_{eff}/\Delta K)$ is the retardation parameter and $(da/dN)_C (= C_0(\Delta K)^m)$ is the crack growth rate under zero-to-tension constant amplitude loading ($R = 0$). According to Matsuoka *et al.* [3], the retardation parameter, U_D, is given by

$$U_D = 1 - (r/2)(1/\omega_B - 1/\omega_D)(a - a_0) \quad \text{for} \quad 0 \leqslant a - a_0 \leqslant \omega_B$$

and

$$U_D = 1 - (r/2)[1 - (1/\omega_D)(a - a_0)] \quad \text{for} \quad \omega_B \leqslant a - a_0 \leqslant \omega_D \quad (2)$$

where a_0 is the crack length at the application of the overload, and ω_B and ω_D are the crack lengths at the minimum growth rate and at the finishing point of retardation, respectively (see Fig. 1). Matsuoka *et al.* [3] gave the size of the overload-affected zone, ω_D, in the case of small scale yielding as

$$\omega_D = 2.5\omega_R^P - \omega_M^1 = [2.5(r/2)^2 - 1]\omega_M^1 \quad (3)$$

* This suggestion was discussed in detail in a later section.

TABLE I (a) Steels

Material	Composition (wt%)											Heat treatment
	C	Si	Mn	P	S	Cu	Ni	Cr	B	V	Mo	
HT80	0.12	0.26	0.96	0.010	0.004	0.19	1.05	0.45	0.002	0.05	0.31	tempered at 550° C
SNCM8	0.40	0.25	0.63	0.029	0.020	0.13	1.68	0.68	–	–	0.18	tempered at 600° C
A553	0.06	0.17	0.54	0.005	0.006	–	9.10	–	–	–	–	as-rolled
SUS304	0.06	0.53	1.11	0.039	0.010	–	9.04	18.29	–	–	–	solution-annealed at 1080° C
SS41	0.17	0.40	0.82	0.014	0.022	–	–	–	–	–	–	as-rolled

TABLE I (b) Aluminium alloys

Material	Composition (wt%)								Heat treatment
	Cu	Si	Fe	Mn	Mg	Zn	Cr	Ti	
A5083-0	0.04	0.13	0.17	0.69	4.53	T_R	0.13	0.01	0
A2017-T3	4.18	0.61	0.32	0.70	0.54	0.194	0.034	–	T3

TABLE I (c) Titanium alloy

Material	Composition (wt%)							Heat treatment
	C	Fe	N	H	O	Al	V	
Ti–6A1–4V	–	0.074	0.0081	0.001	0.171	6.20	4.06	annealed at 820° C

TABLE II

Material	σ_{ys} (MPa)	σ_{yc} (MPa)	m	C_0	γ	$K_{th,0}$ (MPa$\sqrt{m}$)
HT80 steel	784	498	2.22	6.66×10^{-11}	0.71†	7.5†
SNCM8 steel	942	659	2.48	3.61×10^{-11}	0.71	6.2
A553 steel	698	430	1.98	1.55×10^{-10}	0.61†	6.5†
SUS304 steel	336	–	3.32	1.51×10^{-12}	–	–
SS41 steel	270	229	4.34	6.17×10^{-14}	–	–
A5083 A1	143	309	2.92	1.98×10^{-10}	0.55†	3.2†
A2017 A1	322	476	2.76	1.70×10^{-10}	0.55	3.2
Ti–6A1–4V	980	789*	3.02	3.16×10^{-11}	0.71	6.5‡

*: [9].
†: [14, 15].
‡: [16].

where ω_M^1 is the monotonic plastic zone size at the baseline stress and ω_R^P ($= (r/2)^2\omega_M^1$) is the residual plastic zone size left by the overload.

Consequently, the retarded crack growth rate, $(da/dN)_D$, in Equation 1 was expressed as a function of four parameters, r, m, ω_B and ω_D. The stress ratio, r, is prescribed by the test condition, and the exponent parameter, m, is determined by the measurement of fatigue crack growth under zero-to-tension loading. The crack length, ω_D, is given by Equation 3 as a function of r and ω_M^1. The plastic zone size, ω_M^1, could be calculated theoretically. For the case of HT80 steel examined by Matsuoka *et al.* [3], the experimental ω_D values were the same as the theoretical ones when the relevant size, ω_M^1, was computed according to the Dugdale model [8]. However, up to now, the crack length at the minimum growth rate, ω_B, is an unknown factor. In the case of HT80 steel the theoretical curve gave the best fit to the experimental data when $\omega_B = 0.53\omega_R^P$. This model was successfully extended to explain the retardation behaviour of 2024-T3 aluminium alloy examined by von Euw *et al.* [4] and Ti–6A1–4V titanium alloy examined by Wei and Shih [5]. The analytical results showed that $\omega_B = 0.25\omega_R^P$ for aluminium alloy and $\omega_B = 0.53\omega_R^P$ for titanium alloy. Furthermore the experimental value of ω_D for the aluminium alloy was larger than that calculated from Equation 3 on the basis of the Dugdale model. This fact indicates that the overload affected zone size, ω_D, may be dependent on the material or other factors given by loading conditions.

In the present study the delayed retardation phenomena of fatigue crack growth in four steels, two aluminium alloys and a titanium alloy were investigated. The results were analysed according to the model proposed by Matsuoka *et al.* [3]. Then the two crack lengths, ω_B and ω_D, characteristic of the retardation phenomena of these materials, were determined.

2. Experimental procedures

The materials used were four steels, JIS SNCM8, JIS SUS304, JIS SS41 and ASTM A553, two aluminium alloys, A5083-0 and A2017-T3, and Ti–6A1–4V titanium alloy. The three steels, SNCM8, A553 and SS41 were selected as representative of high, medium and low strength steels, respectively. The SUS304 steel was selected because this is of cyclic-hardening type in contrast to the other steels of cyclic-softening type. For comparison, the data for HT80 steel in the previous study [3] were also presented. The chemical compositions of these materials are shown in Table I, and the values of their monotonic and cyclic yield strengths are given in Table II. The cyclic yield strengths, except that of the titanium alloy, were obtained from strain controlling tests on cylindrical specimens with the gauge part 10 mm in diameter and 10 mm in length. The value of cyclic yield strength for the Ti–6A1–4V titanium alloy is referred to that measured by Landgraf *et al.* [9]. It should be noted in Table II that steels (except SUS304 steel) and titanium alloy cyclic-softened, while aluminium alloys cyclic-hardened.

All crack growth studies were carried out under zero-to-tension loading by using centre-cracked specimens (Fig. 2). Cracks were initiated from 4 mm long saw cuts in a 7 mm diameter central hole. The single cycle of overload was run manually at a frequency of 0.1 Hz. The values of the baseline stress, σ_1, and the peak/baseline stress ratio, $r = \sigma_2/\sigma_1$, employed in this test are shown in Table III. In the present study the subscripts

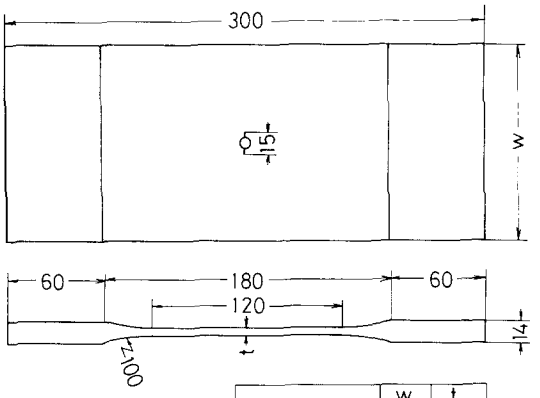

	w	t
HT80 Steel	140	10.0
SNCM8 Steel	75	4.0
A553 Steel	120	3.5
SUS304 Steel	120	5.0
SS41 Steel	120	5.0
A5083 Al	120	8.0
A2017 Al	120	7.0
Ti-6Al-4V	120	5.0

Figure 2 Configuration of centre-cracked specimens (dimensions are given in mm).

1 and 2 designate the values at baseline stress and overload, respectively. The experiments and the analyses of the data were mainly conducted for the case of $r = 2$. In Table III are given the values of the ratio of peak stress to monotonic yield strength, $2\sigma_1/\sigma_{ys}$, relevant to the case of application of overload with $r = 2$. The small scale yielding condition was not satisfied at the overload of $2\sigma_1$ in the tests for SS41 steel, since the pertinent value of $2\sigma_1/\sigma_{ys}$ became 0.73. In the case of SUS304 steel and A5083 aluminium alloy the values of $2\sigma_1/\sigma_{ys}$ lay on the borderline between small scale yielding and large scale yielding. Testing was done on a 15 ton MTS electrohydraulic testing machine with a frequency of 20 Hz. Cycling was interrupted periodically and the increment of crack extension was measured with an optical microscope. In order to examine the fracture surface morphology associated with different materials, appropriate specimens were examined by using a scanning electron microscope.

3. Experimental results

3.1. Crack growth measurement

Fig. 3 represents crack growth rates, $(da/dN)_C$, under constant amplitude zero-to-tension loading for the various materials, against stress intensity range, ΔK. In the calculation of the value of ΔK, the effect of specimen width was corrected by using the secant formula [3, 10]. It is seen from Fig. 3 that the $\log (da/dN)_C$ versus $\log \Delta K$ relationships for steels and the titanium alloy appeared almost linear in the range of testing, while those for the aluminium alloys became concave upward. In Table II are given the values of the parameters C_0 and m in the Paris equation characterizing the crack growth rate for these materials where ΔK and $(da/dN)_C$ have units of MPa $m^{1/2}$ and m $cycle^{-1}$, respectively. The corresponding parameters for aluminium alloys were determined by the linear approximation of the data ranging ΔK from 7.8 to 14.0 MPa $m^{1/2}$ for A5083 aluminium alloy and from 10.9 to 23.2 MPa $m^{1/2}$ for A2017 aluminium alloy, in which the delay experiments were carried out.

Fig. 4a shows the typical behaviour of retardation phenomena in eight materials for the case of a single application of overload with $r = \sigma_2/\sigma_1 = 2$, by plotting the crack length, $a - a_0$, against the number of cycles, N. The relevant crack growth rates, $(da/dN)_C$, at constant amplitude loading in these curves were nearly equal to 1.5×10^{-7} m $cycle^{-1}$ for all materials except SUS304 steel, SS41 steel and the Ti–6Al–4V titanium alloy. In the cases of SUS304 and SS41 steels, the specimens generally yielded when the single overload of $2\sigma_1$ was applied at the baseline stress intensity, ΔK_1, corresponding to the growth rate of $(da/dN)_C = 1.5 \times 10^{-7}$ m $cycle^{-1}$. In the case of the titanium

TABLE III

Material	σ_1 (MPa)	$r = \sigma_2/\sigma_1$	$2\sigma_1/\sigma_{ys}$
HT80 steel	98, 147	1.25, 1.5, 1.625, 1.75, 2.0	0.25, 0.38
SNCM8 steel	98	1.4, 1.6, 1.8, 2.0	0.21
A553 steel	117.6	1.4, 1.6, 1.8, 2.0	0.34
SUS304 steel	88.2	2.0	0.53
SS41 steel	98	1.4, 1.6, 1.8, 2.0	0.73
A5083 Al	39.2	1.4, 1.6, 1.8, 2.0	0.54
A2017 Al	58.8	2.0	0.37
Ti–6Al–4V	98	2.0	0.20

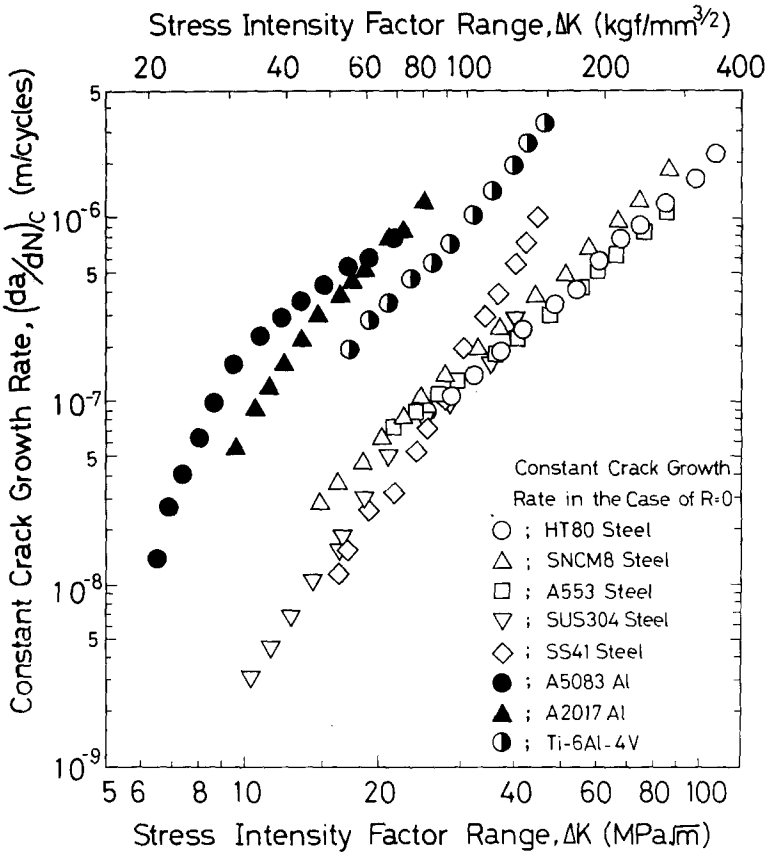

Figure 3 Fatigue crack growth rates under constant amplitude zero-to-tension loading for various materials, against stress intensity range.

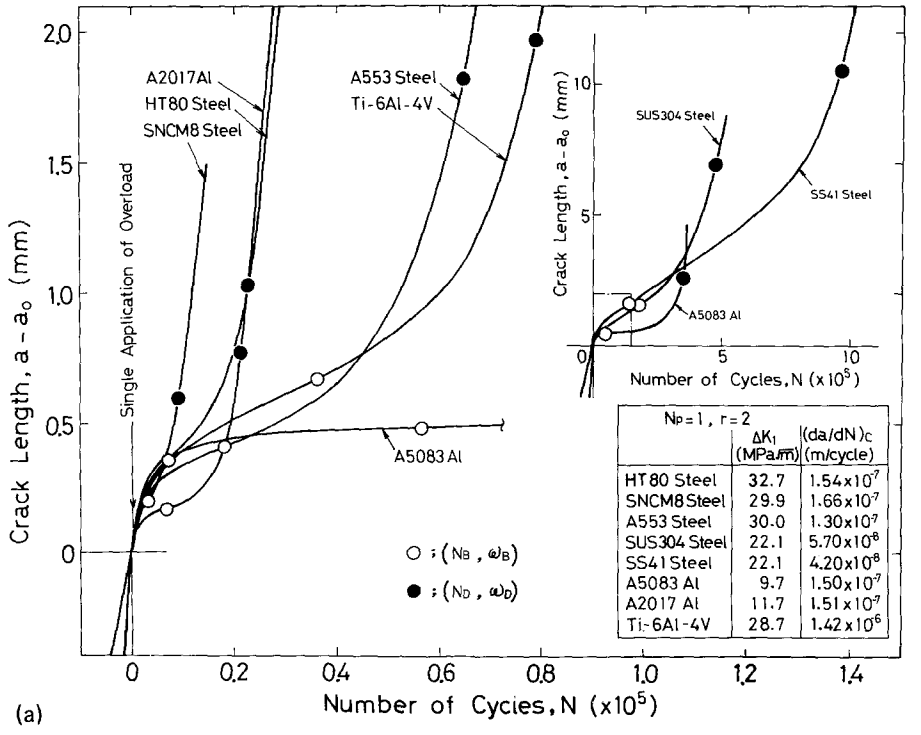

Np = 1, r = 2	ΔK1 (MPa√m)	(da/dN)c (m/cycle)
HT80 Steel	32.7	1.54×10⁻⁷
SNCM8 Steel	29.9	1.66×10⁻⁷
A553 Steel	30.0	1.30×10⁻⁷
SUS304 Steel	22.1	5.70×10⁻⁸
SS41 Steel	22.1	4.20×10⁻⁸
A5083 Al	9.7	1.50×10⁻⁷
A2017 Al	11.7	1.51×10⁻⁷
Ti-6Al-4V	28.7	1.42×10⁻⁶

Figure 4 Typical behaviour of retardation phenomena in eight materials. (a) Relationships of crack length, $a - a_0$, and number of cycles, N.

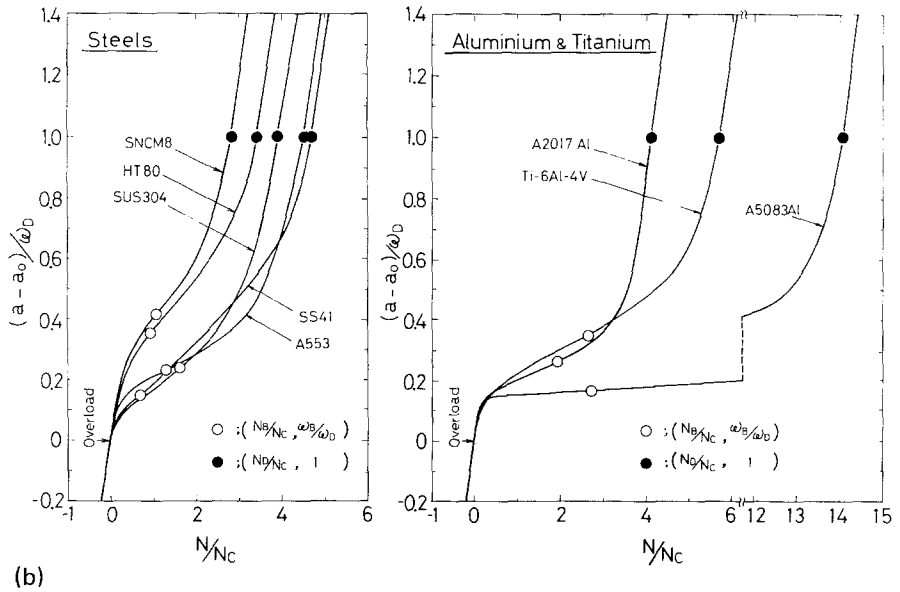

Figure 4 (b) Normalized form of $(a-a_0)/\omega_D$ versus N/N_C.

alloy, the resulting overload-affected zone size, ω_D, was so small that it was impossible to obtain any clear curve of crack length versus number of cycles. Thus, in these cases, the experimental data for $(da/dN)_C \simeq 5 \times 10^{-8}$ m cycle^{-1} in SUS304 and SS41 steels, and $(da/dN)_C = 1.42 \times 10^{-6}$ m cycle^{-1} in the titanium alloy were employed in Fig. 4a. It is seen from Fig. 4a that all the samples exhibited a similar pattern of delayed retardation as illustrated in Fig. 1; the retardation attained a maximum at the inflection points indicated by open circles ($a-a_0=\omega_B$) and disappeared at the points indicated by solid circles ($a-a_0=\omega_D$). This is much clearer in Fig. 4b, where the data in Fig. 4a are replotted in the normalized form of $(a-a_0)/\omega_D$ versus N/N_C. Here N_C is the number of cycles required for propagation through the overload-affected zone at constant growth rate and calculated as $\omega_D/(da/dN)_C$. However, the values of ω_B, ω_D and N_D characterizing the retardation phenomenon depended strongly on material as follows:

(1) The amount of retardation, N_D, increased with increasing overload-affected zone size, ω_D. For example, when the results of HT80 steel were adopted as a standard of comparison, the values of ω_D and N_D for SS41 steel became ten and fifty times as large as those for HT80 steel, respectively. On the other hand, the values of ω_D and N_D for SNCM8 steel, which exhibited the least amount of retardation among the materials tested, each became nearly half of the respective values for HT80 steel. However, as seen in Fig. 4b, the normalized values of retardation, N_D/N_C, differed only by a factor of two between SS41 steel and SNCM8 steel.

(2) The N_D value of A5083 aluminium alloy is smaller than those of SUS304 and SS41 steels, and the N_D value of A2017 aluminium alloy is almost equal to that of HT80 steel. However, when these are compared in the normalized form as shown in Fig. 4b, it is evident that, in general, the retardation took place much more strongly in aluminium alloys than in steels. The strength of retardation in the titanium alloy seemed to be intermediate between those of steels and aluminium alloys.

(3) In the cases of SNCM8, HT80 and A553 steels, the N_D/N_C values increased with decreasing ω_B/ω_D value. The same tendency was valid for the case of the two aluminium alloys. However, this seemed to break down in the case of SUS304 and SS41 steels. Namely, the ω_B/ω_D value of SUS304 steel was almost equivalent to that of A553 steel, while the N_D/N_C value was smaller. The ω_B/ω_D value of SS41 steel was smaller than that of A553 steel, while the N_D/N_C values were almost the same.

3.2. Observation of fracture surface

Fig. 5 represents the macroscopic fractographs of various materials, which were overloaded at the values of ΔK_1 when the corresponding crack growth rates, $(da/dN)_C$, became almost equal. For

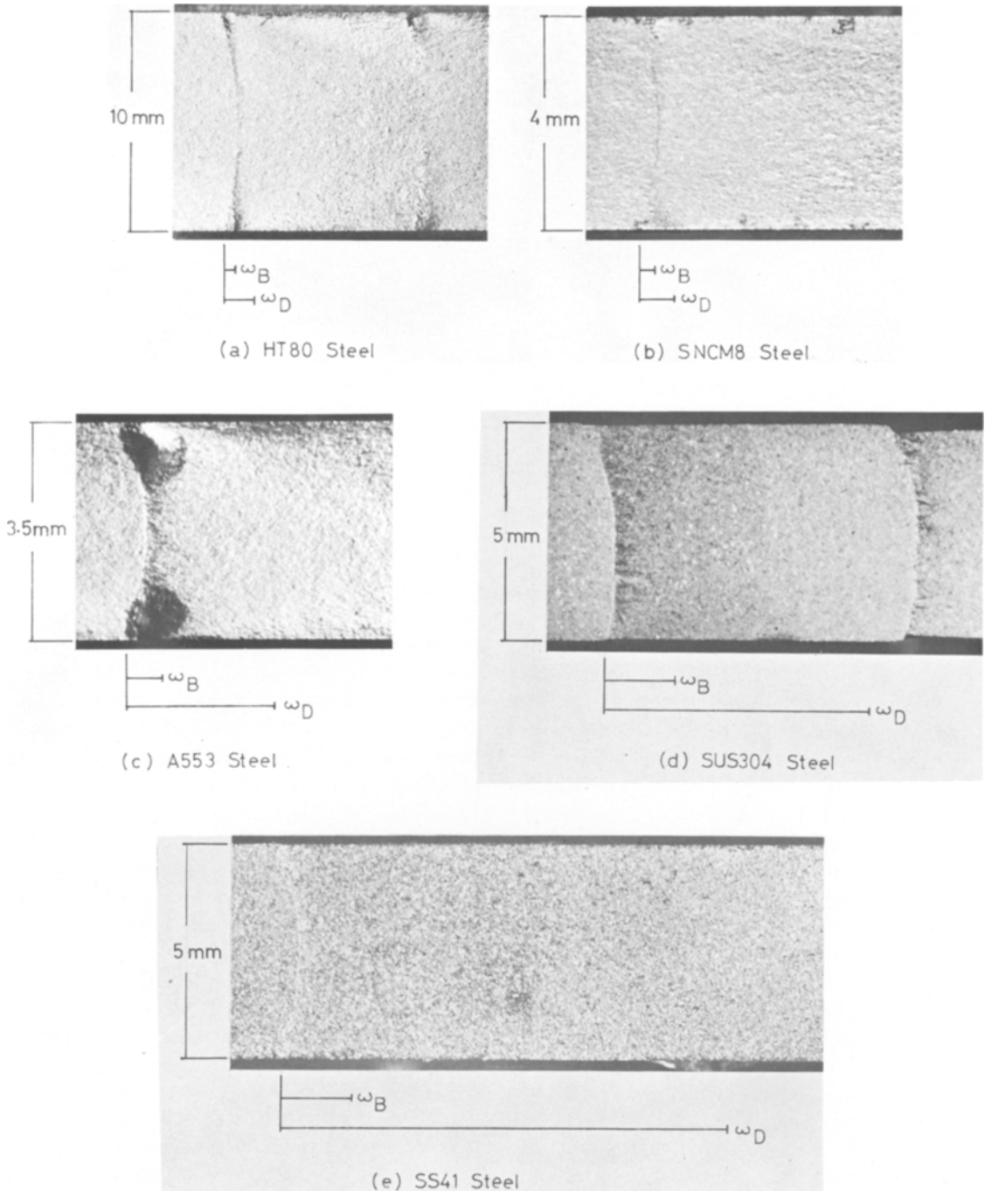

Figure 5 Macroscopic fractographs showing the dark bands relevant to the overload cycle.

convenience of comparison, the photographs of the specimens in Fig. 5 were printed so as to have an identical size of specimen width on the paper. The crack distances from the overloaded tip relevant to ω_B and ω_D in each material are indicated in the figure.

The overload cycle was identified by a dark band on the fracture surface. In the cases of steels excluding SS41 steel, the dark band became better defined as the N_D/N_C value became larger. In SS41 steel, the band was hardly discernible. The band seemed to appear clearer in aluminium alloys

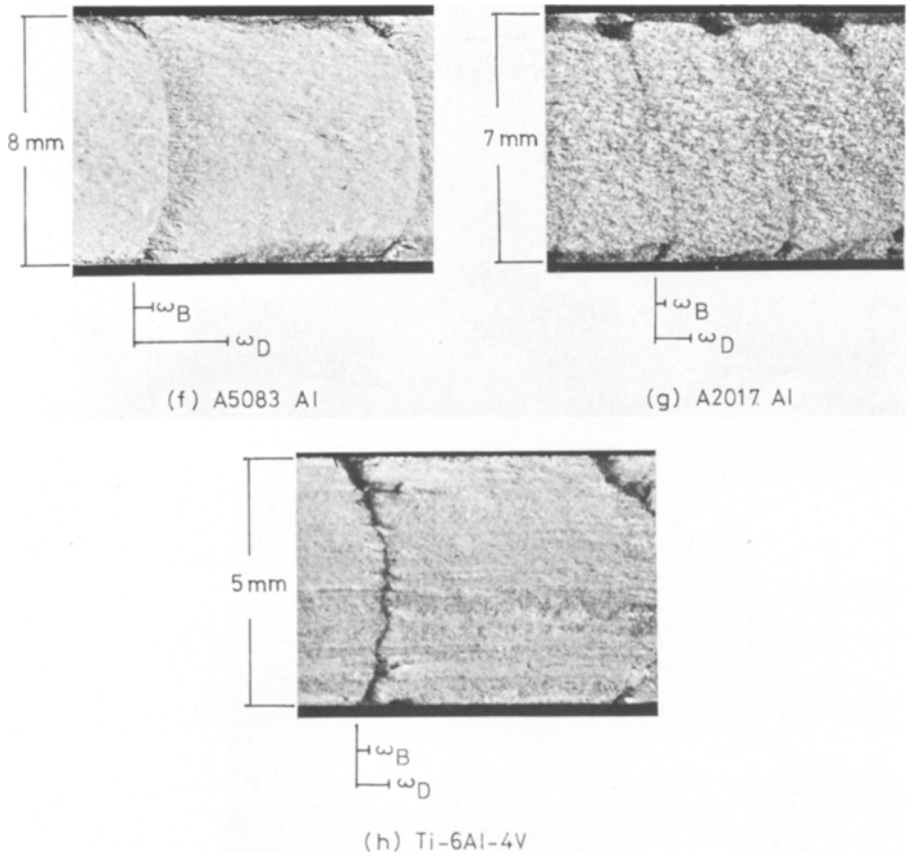

Figure 5 continued.

and titanium alloy than in steels. It should be noted that the sizes of the dark bands in these materials were roughly equal to the distance, ω_B, where the crack growth rate became a minimum.

The dark band was more discernible in the vicinity of the specimen surface than in the interior part of the specimen. In particular, the dark band appeared distinctly in the vicinity of the specimen surface in A553 steel and A2017 aluminium alloy; this was intimately related to the shear lip. That is, after the overload the shear lip rapidly decreased to a smaller size corresponding to the lower growth rates in the retarded region, and then gradually increased to its original value; the darkest mark was formed in the portion of the shear lip decreasing in size.

Scanning electron fractographs revealed that a stretch zone formed at the crack tip during the overload cycle. The stretch band was followed immediately by abrasion (Fig. 6). The amount of abrasion increased as the macroscopic dark band was better defined. The features of abrasion were similar between HT80 steel (Fig. 6a) and A5083 aluminium alloy (Fig. 6b). However, abrasion was not found in the fracture surface in SS41 steel (Fig. 6c), in which the testing condition of small scale yielding was not satisfied.

4. Analysis of results

The slopes of the crack length versus number of cycles curves for the retarded cracks of the various materials will be analysed according to the model proposed by Matsuoka *et al.* [3]. Then, the number of cycles during retardation obtained from the experiments for the materials will be compared with the theoretical ones given by integrating Equation 1.

4.1. Retarded crack growth rate

Fig. 7 shows the ratio of the constant growth rate to the retarded growth rate, $(da/dN)_C/(da/dN)_D$, against the normalized crack length, $(a-a_0)/\omega_0$,

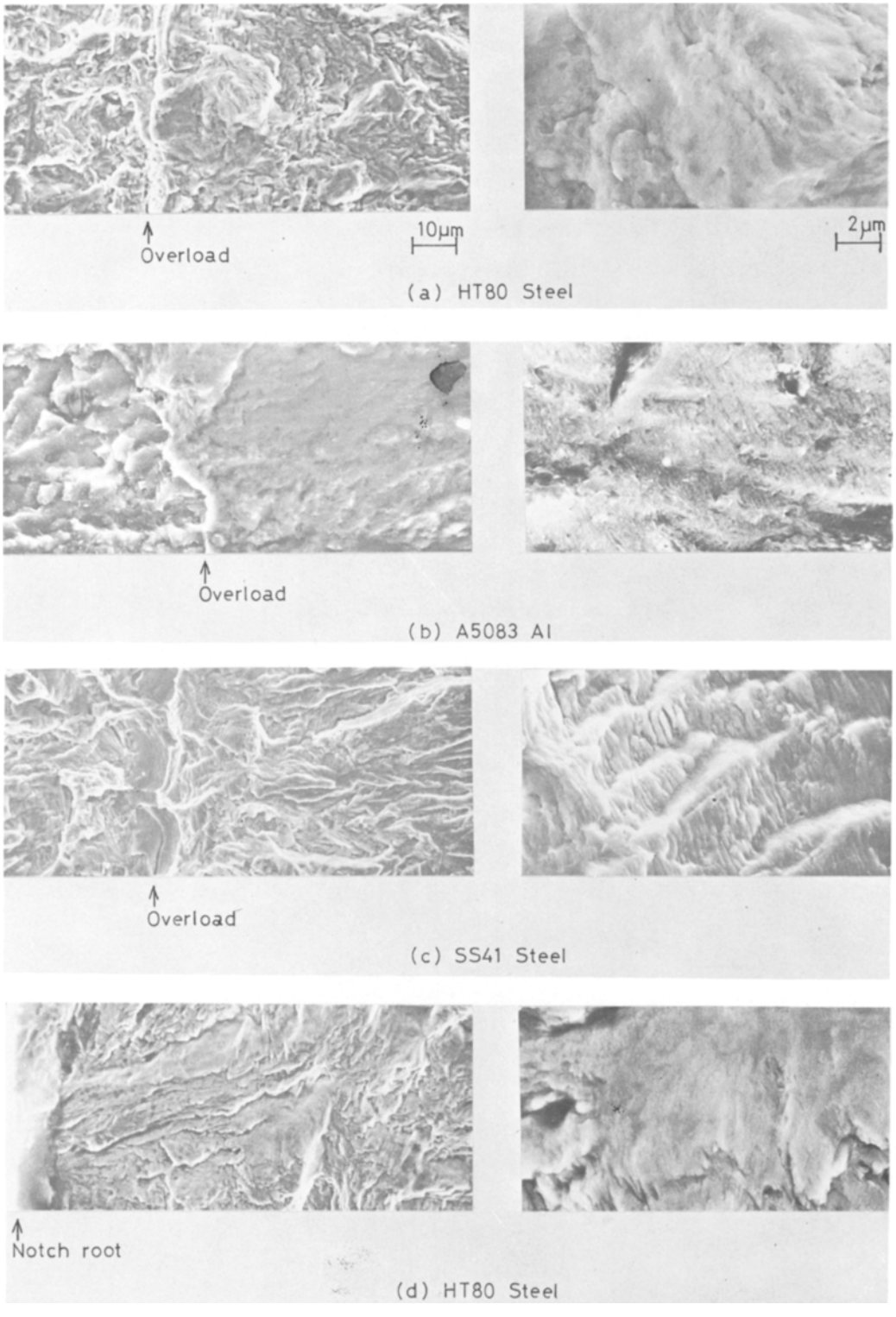

Figure 6 Scanning electron fractographs. Cracks propagated the left side of photographs to the right side. (a) HT80 steel. (b) A5083 aluminium alloy. Note abrasion marks in the dark bands due to overload cycle. (c) SS41 steel. Abrasion is not found in the fracture surface. (d) Fracture surface at a notch root of 5 mm radius in HT80 steel tested under constant amplitude zero-to-compression loading. Note the similarity of the morphology to that of the fracture surface in Fig. 6a.

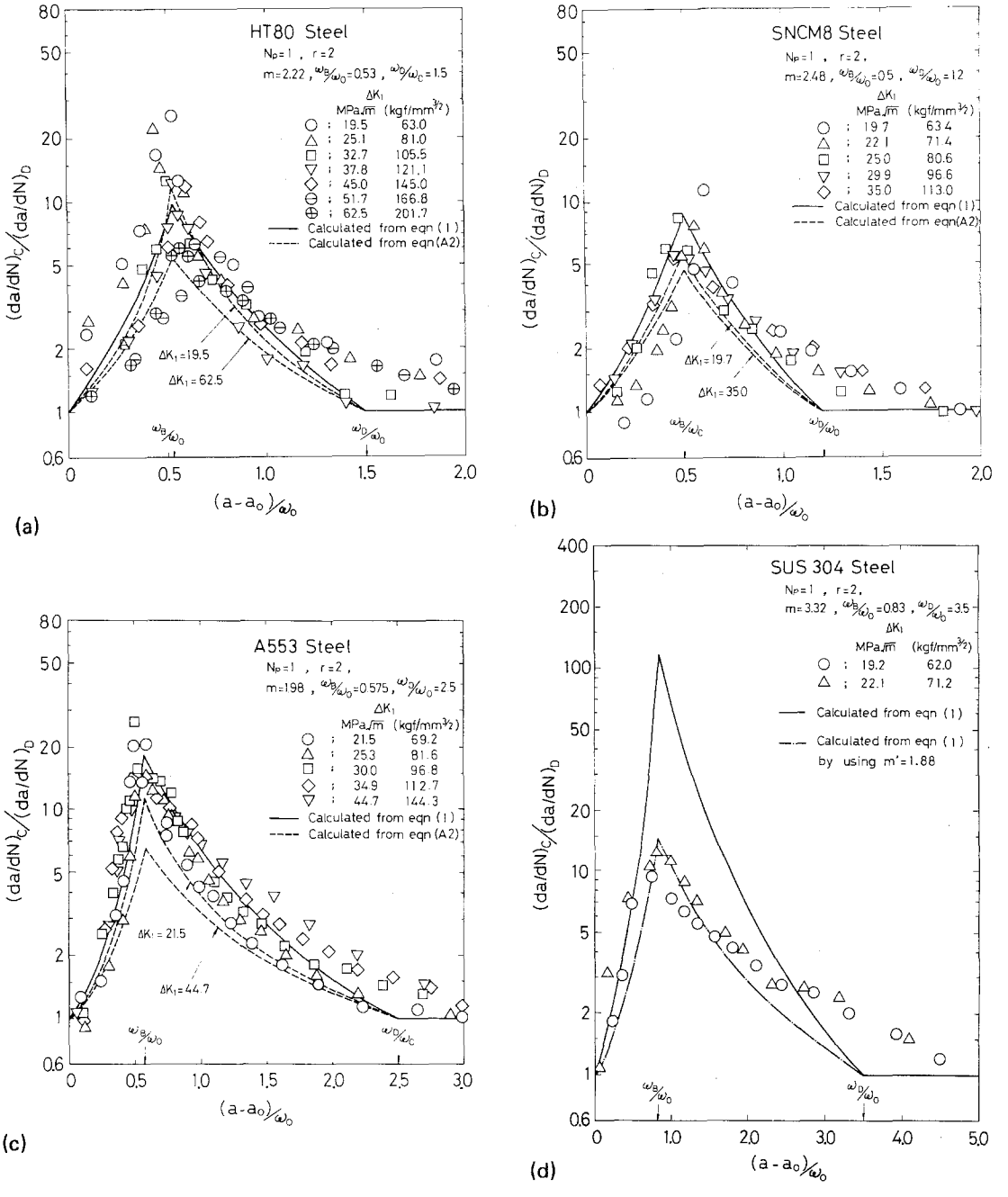

Figure 7 Ratio of constant crack growth rate to retarded crack growth rate, $(da/dN)_C/(da/dN)_D$, as a function of normalized crack length, $(a-a_0)/\omega_D$. (a) HT80 steel. (b) SNCM8 steel. (c) A553 steel. (d) SUS304 steel. (e) SS41 steel. (f) A5083 A1. (g) A2017 A1. (h) Ti–6A1–4V.

as a function of baseline stress intensity, ΔK_1, for the eight materials in the case of a single application of overload with $r = 2$. Here, ω_0 is the monotonic plastic zone size at the baseline stress, which is calculated from the assumption of small scale yielding on the basis of the Dugdale model as

$$\omega_0 = (\pi/8)(K_1/\sigma_{ys})^2, \qquad (4)$$

where σ_{ys} is the monotonic yield strength given in Table I. It is seen in Fig. 7 that the data for each material exhibit an almost identical tendency independent of baseline stress intensity, as a result of plotting in the normalized form. However, the tendency seemed sensitive to material. The ratio, $(da/dN)_C/(da/dN)_D$, can be considered to be representative of the strength of retardation. This

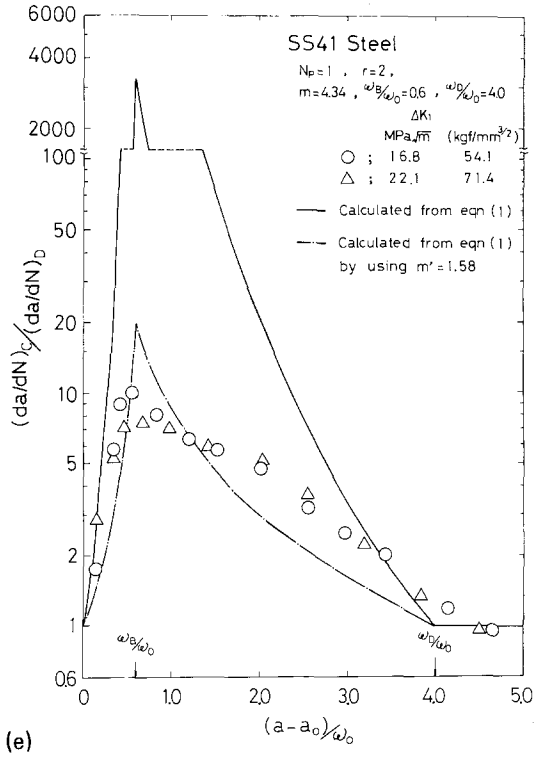

(e)

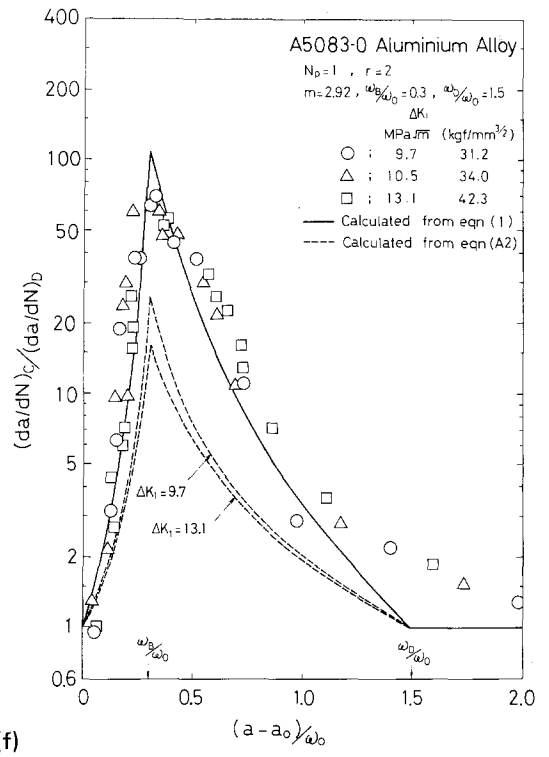

(f)

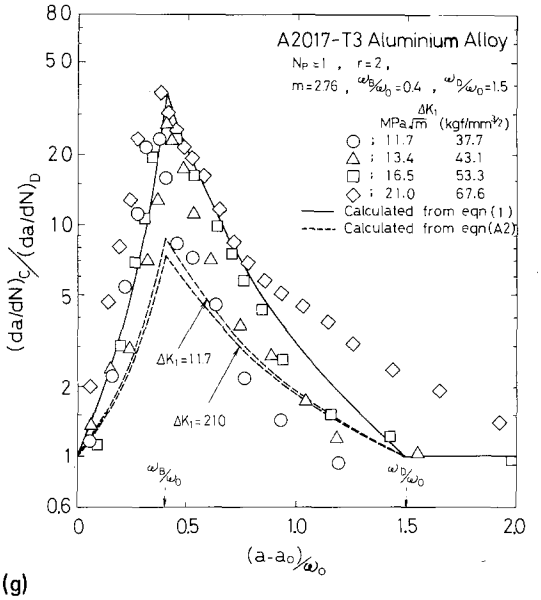

(g)

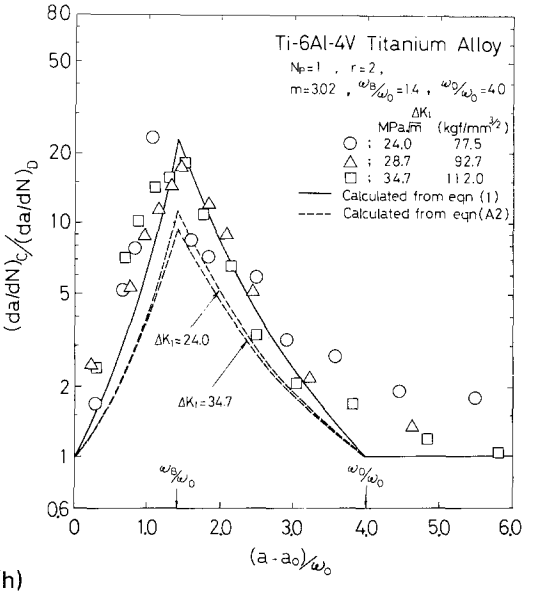

(h)

Figure 7 continued.

ratio should be equal to $(1/U_D)^m$ as deduced from Equation 1. The full curves in Fig. 7 were obtained by substituting the retardation parameter, U_D, in Equation 2 into the expression, $(1/U_D)^m$, where the two crack lengths, ω_B, and ω_D, in Equation 2 were determined so that the theoretical curves gave the best fitting with the experimental data. The resulting values of these crack lengths normalized by the plastic zone size, ω_0, are shown in the insertion of Fig. 7.

It is evident that the theoretical curves indicated by full lines in Fig. 7 agree with the experimental data for the materials tested, when the cases of SS41 and SUS304 steels are excluded. In

the latter cases the theoretical curves overestimated the experimental results. This fact also ties up with the unusual shape of the $(a-a_0)/\omega_D$ versus N/N_C curves in the same materials as shown in Fig. 4b. A better fitting of theory to experiment can be given by changing the value of the exponent, m, to a smaller value than that obtained under constant amplitude loading. The theoretical curves calculated by using a modified exponent, m', for each of SS41 and SUS304 steels were shown by dash-dotted ones in Figs. 7d and e, respectively. The weaker retardation of the two materials than expectation probably occurs because the small scale yielding condition was not satisfied in the testing for SS41 and SUS304 steels. In this situation, the clamping force due to the elastic material surrounding the residual plastic zone will not operate so strongly as that under small scale yielding because the size of the residual plastic zone produced by overload becomes large compared with the width of specimen.

4.2. Amount of retardation

As seen in Figs. 4 and 7, the strength of retardation depended on material, and the dependence of retardation on material was expressible in terms of the ratio, N_D/N_C. Fig. 8 shows the effect of the peak/baseline stress ratio, r, on the amount of retardation, N_D/N_C. It is seen that the retardation increased as the ratio, r, became higher when $r \geqslant 1.4$, and disappeared when $r < 1.4$. The N_D/N_C values were more sensitive to stress ratio, r, in aluminium alloys than in the steels or the titanium alloy. Fig. 9 represents the effect of baseline stress intensity, ΔK_1, on N_D/N_C values for the case of a single application of overload when $r = 2$. The amount of retardation, N_D/N_C, for HT80 steel and Ti–6Al–4V titanium alloy increased with decreasing baseline stress intensity, ΔK_1, while the trend of A2017 aluminium alloy and A553 steel appeared in the reverse direction. The former behaviour is similar to that in the results for the Ti–6Al–4V titanium alloy examined by Wei and Shih [5], and the latter behaviour is similar to that in the results for 2024-T3 aluminium alloy by von Euw *et al.* [4]. The behaviour of ΔK_1 dependence of retardation in SNCN8 steel seemed to be the combination of the two different behaviours mentioned above; decreasing ΔK_1 below 15 MPa $m^{1/2}$ caused an increase in N_D/N_C

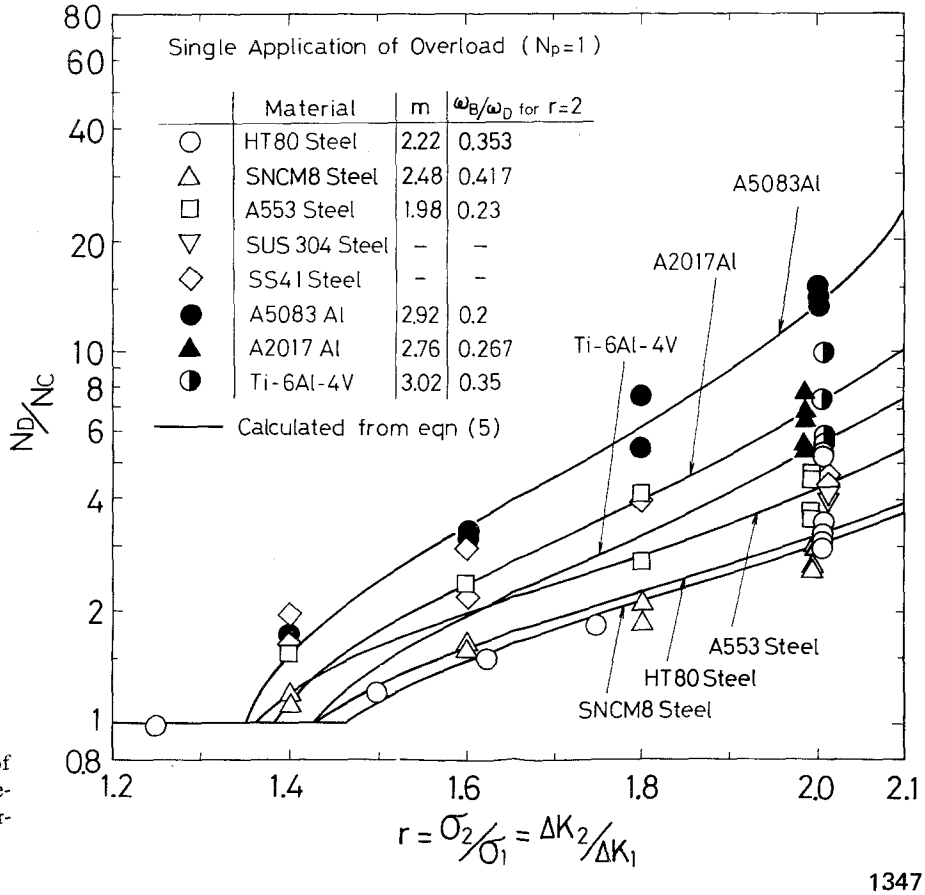

Figure 8 Effect of ratio of peak to baseline stress on retardation.

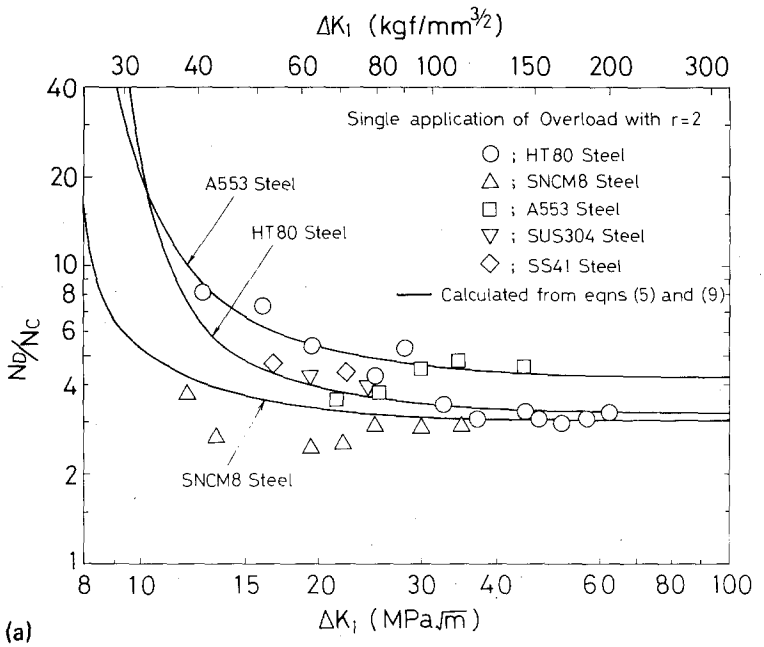

(a)

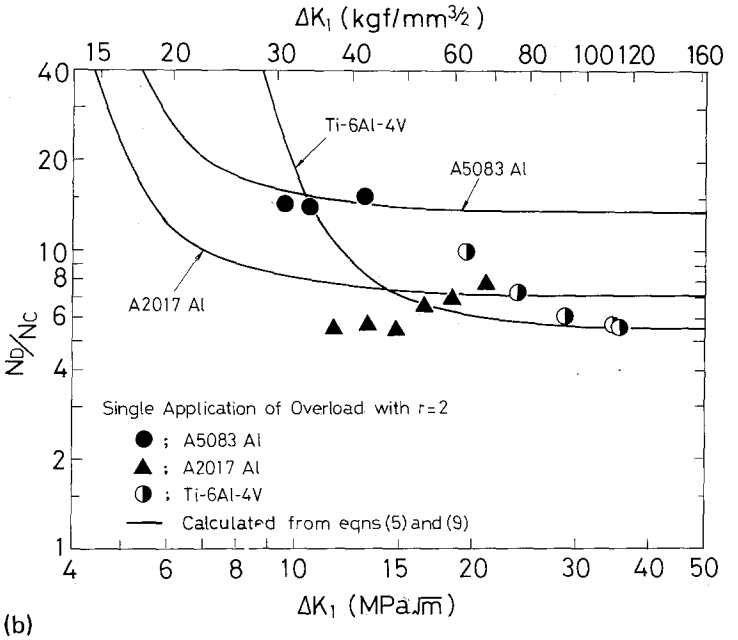

(b)

Figure 9 Effect of baseline stress intensity range on retardation ($r = 2$).

value, and increasing ΔK_1 above this level caused an increase in N_D/N_C value, although the dependence on ΔK_1 was moderate. This similar feature of dependence on ΔK_1 was shown in 2014-T3 aluminium alloy tested by Crandall and Hillberry [7].

The amount of retardation, N_D/N_C, can be estimated by substituting Equation 2 into Equation 1 and integrating from $a = a_0$ to $a = a_0 + \omega_D$, as follows;

$$N_D/N_C = (1/\omega_D)\int_{a_0}^{a_0+\omega_D} (da/dN)_C/(da/dN)_D da$$
$$= \{[1-(r/2)(1-\omega_B/\omega_D)]^{1-m} - 1\}/[(m-1)(r/2)(1-\omega_B/\omega_D)]. \quad (5)$$

The full curves in Fig. 8 are the theoretical ones which were calculated from Equation 5 by using the values of m and ω_B/ω_D for each material as indicated in the insertion of Fig. 8. In the case

when the stress ratio, r, became lower than two, the N_D/N_C value was calculated from Equation 5 together with Equation 3 under the assumption that the ω_B/ω_R^P value was constant and equal to that for the case of $r = 2$. That is, $\omega_B/\omega_D = (\omega_B/\omega_R^P)(\omega_R^P/\omega_D) = (\omega_B/\omega_R^P)/[2.5 - (2/r)^2] = (\omega_B/\omega_R^P)_{r=2}/[2.5 - (2/r)^2]$. The calculation for those of SUS304 and SS41 steels was not conducted because the small scale yielding condition was not satisfied in these cases. Equation 5 indicates that N_D/N_C increases with increasing r and m and with decreasing ω_B/ω_D. It is apparent in Fig. 8 that the theoretical curves explain satisfactorily the main features of the dependence of retardation on the peak/baseline stress ratio, r.

The results in Fig. 8 demonstrate the dependence of retardation on material. This is reflected in the two parameters, m and ω_B/ω_D. The comparison of the results of HT80 steel and Ti–6A1–4V titanium alloy shows that the difference in retardation behaviour is mainly due to a difference in the exponent parameter, m, since both materials have an almost identical value of ω_B/ω_D. The difference in retardation between A5083 aluminium alloy and Ti–6A1–4V titanium alloy shows the effect of the parameter, ω_B/ω_D, since the exponent parameters, m, for both materials are almost equal. As can be found from the formulation in Equation 5 and from the results in Figs. 4b and 7, the exponent parameter m only changes the magnitude of retardation, while the parameter ω_B/ω_D affects the character of retardation as well as its magnitude.

5. Discussion

The crack growth rates following a single overload for materials employed in this study were expressed by Equation 1 as long as the small scale yielding condition was satisfied. The values of three parameters, m, ω_B/ω_0 and ω_D/ω_0, characterizing the retardation phenomena, were described in Fig. 7 for each material. In the following, the dependence of ω_B/ω_0 value on material and the relationship between ω_D/ω_0 value and stress state at the crack tip will be discussed. Furthermore, the relationship between the retardation behaviour and the threshhold value of stress intensity will be considered.

5.1. Dependence of ω_B/ω_0 value on material

The ω_B/ω_0 value would be affected by the aspect of crack blunting induced by the application of overload. The crack blunting may destroy the crack-closing system, which has been established on the crack tip under constant amplitude loading before the application of the overload. As the crack propagates into the residual compressive zone developed by the overload, the new crack-closing system will build up on the crack surface in the wake of the advancing crack front. The model proposed by Matsuoka *et al.* [3] suggests that the stress ratio of the equivalent loading system in the subsequent crack growth just after the overload cycle is negative. Thus, this situation is analogous to that of a crack propagating from a slit or notch under the negative stress ratio of constant amplitude loading. Evidence for this analogy is the presence of abrasion showing rubbing of the fracture surfaces formed after the stretch band made by the overload (Fig. 6). Similar abrasion occurred in the fracture surface at the root of a notch examined under negative stress ratio loading, as shown in Fig. 6d. The photograph is a scanning electron microfractograph revealing abrasion, which appeared on a fracture surface at a notch root of 5 mm radius in HT80 steel tested under zero-to-compression loading. In the latter testing the crack stopped propagating at a distance from the surface of the notch root corresponding to the order of cyclic plastic zone size produced at the notch root [11].

Consequently, it is considered that the ω_B/ω_0 value in retardation testing would reflect the ability of producing tensile residual displacements on the crack surface. In other words, the overload crack tip becomes closed more rapidly in the material with the smaller value of ω_B/ω_0. It is likely that the ω_B/ω_0 value is related to the cyclic deformation resistance of material, and that the value for cyclic-hardening material is smaller than that of cyclic-softening material. It is indicated in Table II that aluminium alloys cyclically-hardened, while steels and titanium alloy cyclically-softened, In accordance with these cyclic behaviours, the values of ω_B/ω_0 for aluminium alloys were smaller than those for steels and titanium alloy, as shown in Fig. 7. Furthermore, from the analogy to a crack at a notch root, the size of ω_B would be comparable with the size of the cyclic plastic zone under baseline loading testing, when the crack tip was blunted completely by the overload cycle. Thus, in the case when $r = 2$, ω_B/ω_0 is roughly equal to 0.25, since the cyclic plastic zone size is evaluated from Equation 4 by equating

σ_{ys} to $2\sigma_{ys}$. This value is nearly equal to those for aluminium alloys. However, of course, the suggestion mentioned above is not sufficient for the complete justification of the sensitive dependence of ω_B/ω_0 on material. More refined theory will be required for the solution of this problem.

5.2. Dependence of ω_D/ω_0 value on material and baseline stress intensity

The overload-affected zone size, ω_D/ω_0, is predicted from Equations 3 and 4 to be equal to 1.5 for the case of $r = 2$. For HT80 steel and A5083 aluminium alloy the retardation almost disappeared at the expected value of $\omega_D/\omega_0 = 1.5$, as shown in Fig. 7. However, the ω_D/ω_0 values for SNCM8 steel appeared slightly smaller than the expected ones, while those for the Ti–6A1–4V titanium alloy were considerably larger than the expected ones. The values for A2017 aluminium alloy were strongly dependent on the baseline stress intensity, ΔK_1, and varied from 1.05 to 2.0. The values for A553 steel also depended on ΔK_1 and ranged from 2.2 to 3.3, which were considerably larger than the theoretical values. The dependence of ω_D/ω_0 value on ΔK_1 for the latter two materials directly affects the dependence of N_D/N_C on ΔK_1, as shown in Fig. 9. For instance, N_D/N_C values for A2017 aluminium alloy are calculated from Equation 5 to be equal to 4.1 for $\omega_D/\omega_0 = 1.05$ ($\Delta K_1 = 11.7\,\mathrm{MPa\,m^{1/2}}$) and 11.35 for $\omega_D/\omega_0 = 2.0$ ($\Delta K_1 = 21\,\mathrm{MPa\,m^{1/2}}$). These calculated values for N_D/N_C are nearly the same as the experimental ones in Fig. 9.

It is likely that the dependence of ω_D/ω_0 values on the baseline stress intensity, ΔK_1, will be related to the change in the state of stress at the crack tip from plane strain to plane stress. Mills *et al.* [6] studied the effect of specimen thickness on retardation in 2024-T3 aluminium alloy, and they suggested that the magnitude of retardation was influenced by the degree of through-thickness constraint (i.e. plane stress versus plane strain). The standard requirement for plane strain under conditions of monotonic loading is given by

$$2.5\,(K/\sigma_y)^2 \leqslant T \qquad (6)$$

where K is the peak stress intensity and σ_y is the yield strength, and T is specimen thickness [12].

If the peak stress intensity, $r\Delta K_1$, at the overload cycle under zero-to-tension loading satisfies the requirement in Equation 6, the retardation will take place under plane strain, since the residual plastic zone fulfils the plane strain requirement automatically. This condition may be obtained by substituting $K = r\Delta K_1$ and $\sigma_y = \sigma_{ys}$ into Equation 6. If the residual plastic zone produced by overload does not satisfy the plane strain requirement, the retardation will occur predominantly under plane stress as ΔK_1 departs from the corresponding value. This condition may be obtained by substituting $K = r\Delta K_1$ and $\sigma_y = 2\sigma_{ys}$ into Equation 6 and changing the inequality sign in the reverse direction. The retardation in the intermediate region of ΔK_1 between the two critical values will exhibit transitional behaviour from plane strain to plane stress. In summary, these conditions are expressed by

$$\begin{aligned} &2.5\,(\Delta K_1/\sigma_{ys})^2/T \leqslant 1/r^2; && \text{plane strain,} \\ &1/r^2 < 2.5\,(\Delta K_1/\sigma_{ys})^2/T \leqslant 4/r^2; && \text{transition from plane strain to plane stress.} \\ &2.5\,(\Delta K_1/\sigma_{ys})^2/T > 4/r^2; && \text{plane stress.} \end{aligned} \qquad (7)$$

In order to eliminate the effect of specimen thickness, the data in Fig. 9 are replotted in Fig. 10 by using a new parameter, $2.5\,(\Delta K_1/\sigma_{ys})^2/T$. The plane stress and plane strain requirements in Equation 7 are also indicated in the figure ($r = 2$). The general trend of these data shows the presence of a minimum N_D/N_C value in the transition region from plane strain to plane stress conditions; $0.25 \leqslant 2.5\,(\Delta K_1/\sigma_{ys})^2/T \leqslant 1.0$. The increase in the N_D/N_C value in the plane stress region with increase in the parameter can be attributed to the increase in ω_D/ω_0 value with increasing ΔK_1. This is typically shown in the data for A2017 aluminium alloy in Fig. 7 (it is noted that since the ω_B/ω_0 value is almost constant independently of ΔK_1, the ω_B/ω_D value decreases as ΔK_1 increases). This behaviour was also associated with the transition of fracture modes from flat- to shear-type as shown in Fig. 5.

It is probable that the steep rise of the curve in Fig. 10 in the plane strain range results from the increase in the value of exponent, m, along with the approach of the $\log(\mathrm{d}a/\mathrm{d}N)_C$–$\log \Delta K$ curve to the threshold level. This is discussed in the following section.

5.3. Correlation of retardation with threshold of stress intensity

The crack growth rates under constant amplitude loading are influenced by the applied stress ratio,

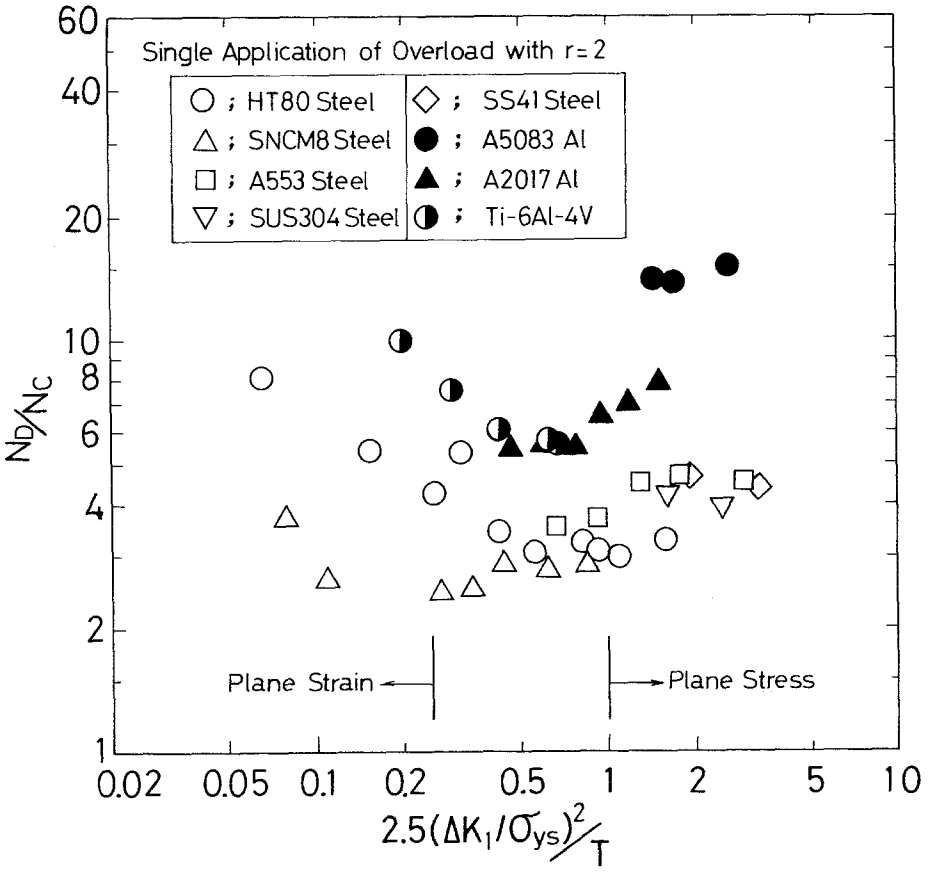

Figure 10 Dependence of N_D/N_C value on parameter, 2.5 $(\Delta K_I/\sigma_{ys})/T$, $(r = 2)$.

R ($\equiv \sigma_{min}/\sigma_{max}$), and the threshold of stress intensity range, ΔK_{th}. On the basis of the crack growth equation proposed by Klesnil and Lukas [13], Ohta *et al.* [14] at the National Research Institute for Metals suggested that the growth rate under constant amplitude loading, $(da/dN)_C$, at the stress ratio of R, was expressed by

$$(da/dN)_C = C_0(1-R)^{-\gamma m}[\Delta K^m - (1-R)^{\gamma m}(\Delta K_{th,0})^m] \quad \text{for} \quad -1 \leqslant R \leqslant 0.33 \tag{8}$$

where γ is a parameter characterizing the effect of stress ratio, R, and $\Delta K_{th,0}$ is the threshold of stress intensity range for $R = 0$. These values for the materials used in the present study are summarized in Table II. The exponent, m, in Equation 8 was assumed to be equal to the value measured in the linear portion of the log $(da/dN)_C$–log ΔK curve in Fig. 3. The values of γ and $\Delta K_{th,0}$ for HT80 steel, A553 steel and A5083 aluminium alloy were those measured by Ohta *et al.* [14, 15]. The results by Klensil and Lukas [13] for three steels with carbon contents, 0.04, 0.12 and 0.65 wt% gave identical values of γ and $\Delta K_{th,0}$, which were equal to 0.71 and 5 MPa $m^{1/2}$, respectively. By referring to the data of steels after Ohta *et al.* [14, 15] and Klensil and Lukas [13], the values of γ and $\Delta K_{th,0}$ for SNCM8 steel were assumed to be equal to 0.71 and 6.2 MPa $m^{1/2}$, respectively. The values for A2017 aluminium alloy were assumed to be the same as those for A5083 aluminium alloy. For titanium alloy, it was assumed that the value of γ was the same as those for steels and that the value of $\Delta K_{th,0}$ was equal to 6.5 MPa $m^{1/2}$ [16].

According to the model developed by Matsuoka *et al.* [3], the effect of residual compressive stress resulting from an overload can be taken into account by assuming an equivalent cyclic loading system. Thus, the retarding crack growth rate, $(da/dN)_D$, would be estimated from the crack growth rate under constant loading sequence with the stress ratio of R equivalent to R_e, where R_e is derived from the relationship between monotonic and cyclic plastic zone sizes produced at the over-

loaded crack tips. That is, the crack growth rate in the equivalent stress system would be affected by the parameter, γ, and the threshold value of stress intensity according to the formulation in Equation 8. The data in Fig. 7 were analysed by following this hypothesis as shown in the Appendix. The results were given by dotted curves in the same figure. It was revealed that the hypothesis may not be correct, since the dotted curves in Fig. 7 were situated considerably lower than the experimental data. The full curves, being based on the simple formulation in Equation 1, gave much better fit with the experimental data. This suggests that the crack closure behaviour during retardation is not identical to that under constant amplitude loading with the corresponding equivalent stress ratio. This may indicate that the crack closure behaviour operating at the corresponding baseline stress intensity would critically affect the crack closure behaviour during retardation.

The dependence of crack closure behaviour on ΔK under constant amplitude is reflected in the exponent parameter, m, in the Paris equation [17]. Therefore, it is conceived that the dependence of retardation on ΔK_1 in the plane strain region in Fig. 10 was related to the change in exponent parameter, m, in the vicinity of the threshold stress intensity. The instantaneous exponent, $m(\Delta K)$, can be expressed by the slope of the tangent to the $\log (\mathrm{d}a/\mathrm{d}N)_C$–$\log \Delta K$ curve at a relevant value of ΔK. In the case of zero-to-tension testing, this is given by differentiating Equation 8 as

$$m(\Delta K) = \mathrm{d}[\log (\mathrm{d}a/\mathrm{d}N)_C]/\mathrm{d}(\log \Delta K)$$
$$= m/[1 - (\Delta K_{th,0}/\Delta K)^m]. \quad (9)$$

The full curves indicated in Fig. 9 are the theoretical relationships between N_D/N_C and ΔK_1 for the materials, which were calculated from Equation 5 by using the instantaneous exponent at ΔK_1 as evaluated in Equation 9 and the values of ω_B/ω_D as shown in Fig. 8. The theoretical curves explain satisfactorily the tendencies in the dependence of N_D/N_C on ΔK_1.

6. Conclusions

The retardation phenomena of fatigue crack growth resulting from a single application of overload were investigated for five steels, JIS HT80, JIS SNCM8, JIS SS41, JIS SUS304 and ASTM A553, two aluminium alloys, A5083 and A2017, and a Ti–6Al–4V titanium alloy under zero-to-tension loading. The data obtained were analysed according to a model proposed by Matsuoka *et al.* [3]. The main conclusions obtained are as follows:

(1) All materials employed in this experiment exhibited delayed retardation. The observed crack growth rates during retardation for these materials, excluding SUS304 and SS41 steels, were expressed theoretically by using four parameters; the peak/baseline stress ratio, r, the exponent in the Paris equation, m, and two crack distances, ω_B and ω_D. The retardation increased with increasing r and m, and with decreasing ω_B/ω_D. However, the retardation in SUS304 and SS41 steels did not occur as strongly as was expected from the model due to Matsuoka *et al.* [3]. This exceptional behaviour can be attributed to the fact that the small scale yielding condition was not satisfied in SUS304 and SS41 steels.

(2) The ω_B/ω_0 values, which show the effect of the crack blunting due to overload, were equal to about 0.5 for steels, 0.3 for A5083 aluminium alloy, 0.4 for A2017 aluminium alloy and 1.4 for Ti–6Al–4V titanium alloy, respectively. This indicates that the cyclic-softening materials have larger ω_B/ω_0 values than the cyclic-hardening materials.

(3) The retardation in HT80 steel and aluminium alloys almost disappeared at the value of $\omega_D/\omega_0 = 1.5$ calculated on the basis of the Dugdale model for the case of $r = 2$. However, the ω_D/ω_0 value for SNCM8 steel was slightly smaller than 1.5 and the values for A553 steel and Ti–6Al–4V titanium alloy were considerably larger than 1.5. Furthermore, the values for A553 steel and A2017 aluminium alloy increased with increasing baseline stress intensity range, resulting in an increase in the amount of retardation. It was believed that such behaviour was related to the change in the stress state from plane strain to plane stress at the crack tip.

(4) In the case of HT80 steel and Ti–6Al–4V titanium alloy, the normalized retardation, N_D/N_C, increased as the baseline stress intensity range decreased. The dependence was explained in connection with the threshold of the stress intensity of the material.

Appendix

Evaluation of crack growth rate during retardation by taking into account the parameter γ and the threshold value

According to the model proposed by Matsuoka

et al. [3], the effect of residual compressive stress produced by overload on retardation can be evaluated by introducing an equivalent cyclic loading system. In the case of zero-to-tension loading, the equivalent stress ratio, R_e, becomes negative. Equation 2 was derived by assuming that the stress intensity effective for crack growth, $K_{eff} = U_D \Delta K_1$, is identical to the maximum stress intensity, $K_{max} = \Delta K_1/(1-R_e)$, in the equivalent cyclic loading system. This results in the following equation:

$$U_D = 1/(1-R_e). \quad \text{(A1)}$$

Now it is assumed that the retarding crack growth rate, $(da/dN)_D$, is equal to the crack growth rate under constant loading sequence with stress ratio R equivalent to R_e. $(da/dN)_D$ can be given by substituting Equation A1 into Equation 8 as

$$(da/dN)_D = C_0(U_D)^{\gamma m}[(\Delta K_1)^m - (U_D)^{-\gamma m}(\Delta K_{th,0})^m]. \quad \text{(A2)}$$

This equation is the generalized form of the formulation in Equation 1, which would include, if ever, the effect of threshold of stress intensity factor and the parameter, γ. The dotted curves in Fig. 7 are the theoretical ones for the materials which were calculated from Equation A2 by using the values given in Table II. The upper and lower dotted curves are the limits relevant to the maximum and minimum values of the baseline stress intensity, respectively, for each material. The dotted curves in Fig. 7 estimated the experimental data considerably lower.

Another disadvantage in this theory lies in the prediction of the value of ΔK_1, when complete arrest of crack propagation would occur. The critical value can be obtained from Equation A2 under a condition, $(da/dN)_D = 0$; i.e., $(\Delta K_1)_{crit} = \Delta K_{th,0}/(U_D)^{\gamma}$. Since the minimum value of U_D is equal to ω_B/ω_D at $r = 2$ [3], the critical value of ΔK_1 becomes

$$(\Delta K_1)_{crit} = (\omega_D/\omega_B)^{\gamma}\Delta K_{th,0}. \quad \text{(A3)}$$

For example, in the case of HT80 steel, the value of $(\Delta K_1)_{crit}$ is calculated as 15.7 MPa m$^{1/2}$ from Equation A3 by using the appropriate values indicated in Fig. 7 and Table II. The experimental data in Fig. 9a shows that crack arrest did not take place by the application of overload of ΔK_1 less than the predicted critical value.

Acknowledgement

The data used in this study are based on the research works contracted between N.R.I.M. and the following companies; Nippon Kokan K. K., Sasebo Heavy Industries Co. and Nippon Steel Co. Particular thanks are due to Dr M. Kawahara in Nippon Kokan K. K. The able assistance of K. Kouze and M. Miyazawa in conducting the fatigue testing and the drafting is also acknowledged.

References

1. J. SCHIJVE, Rep. MP195, National Luchtvaart Lavoratorium, Amsterdam (1960).
2. W. ELBER, ASTM Spec. Tech. Pub. No. 486 (1971) 230.
3. S. MATSUOKA, K. TANAKA and M. KAWAHARA, *Eng. Fracture Mech.* 8 (1976) 507.
4. E. F. J. von EUW, R. W. HERTZBERG and R. ROBERTS, ASTM Spec. Tech. Pub. No. 513 (1972) 230.
5. R. P. WEI and T. T. SHIH, *Int. J. Fracture* **10** (1974) 77.
6. W. J. MILLS and R. W. HERTZBERG, *Eng. Fracture Mech.* 7 (1975) 705.
7. G. M. CRANDALL and B. M. HILLBERRY, Proceedings of the Fourth International Conference on Fracture, Waterloo, Canada, Vol. 2 (1977) p. 1009.
8. D. S. DUGDALE, *J. Mech. Phys. Solids* 8 (1960) 100.
9. R. W. LANDGRAF, JeDEAN MORROW and T. ENDO, *J. Mater.* 4 (1969) 176.
10. R. E. FEDDERSEN, ASTM Spec. Tech. Pub. No. 410 (1966) 77.
11. S. MATSUOKA and K. TANAKA, Preprints of JSME (in Japanese) (1977).
12. G. T. HAHN, R. G. HOAGLAND and A. R. ROSENFIELD, *Met. Trans.* 3 (1972) 1189.
13. M. KLESNIL and P. LUKAS, *Mater. Sci. Eng.* 9 (1972) 231.
14. A. OHTA and E. SASAKI, *Eng. Fracture Mech.* 9 (1977) 307.
15. *Idem*, Preprints of JSME (in Japanese) (1977).
16. R. J. BUCCI, P. C. PARIS, R. W. HERTZBERG, R. A. SCHMIDT and A. F. ANDERSON, ASTM Spec. Tech. Pub. No. 513 (1972) 125.
17. K. TANAKA and S. MATSUOKA, *Int. J. Fracture* **13** (1977) 563.

Received 30 September and accepted 19 October 1977.